Route to Renewable PET: Reaction Pathways and Energetics of Diels−Alder and Dehydrative Aromatization Reactions Between Ethylene and Biomass-Derived Furans Catalyzed by Lewis Acid Molecular Sieves

Joshua J. Pacheco,[†,§] Jay A. Labinger,[†] Alex L. Sessions,[‡] and Mark E. Davis*,[†]

[†]Division of Chemistry and Chemical Engineering, [‡]Division of Geological and Planetary Sciences, California Institute of Technology, Pasadena, California 91125, United States

S *Supporting Information*

ABSTRACT: Silica molecular sieves that have the zeolite beta topology and contain framework Lewis acid centers (e.g., Zr-β, Sn-β) are useful catalysts in the Diels−Alder and dehydrative aromatization reactions between ethylene and various renewable furans for the production of biobased terephthalic acid precursors. Here, the main side products in the synthesis of methyl 4-(methoxymethyl)benzene carboxylate that are obtained by reacting ethylene with methyl 5-(methoxymethyl)-furan-2-carboxylate are identified, and an overall reaction pathway is proposed. Madon−Boudart experiments using Zr-β samples of varying Si/Zr ratios clearly indicate that there are no transport limitations to the rate of reaction for the synthesis of p-xylene from 2,5-dimethylfuran and ethylene and

strongly suggest no mass transport limitations in the synthesis of methyl p-toluate from methyl 5-methyl-2-furoate and ethylene. Measured apparent activation energies for these reaction-limited systems are small (<10.5 kcal/mol), suggesting that apparent activation energies are derived from a collection of parameters and are not true activation energies for a single chemical step. In addition, ^{13}C kinetic isotope effects (KIE) in the synthesis of MMBC and MPT measured by gas chromatography/isotope-ratio mass spectrometry in reactant-depletion experiments support the Madon−Boudart result that these systems are not transport-limited and the KIE values agree with those previously reported for Diels−Alder cycloadditions.

KEYWORDS: *terephthalic acid, dimethyl terephthalate, ethylene, 5-(hydroxymethyl)furfural, Diels−Alder cycloaddition, dehydration, zirconium-β, tin-β, kinetic isotope effect*
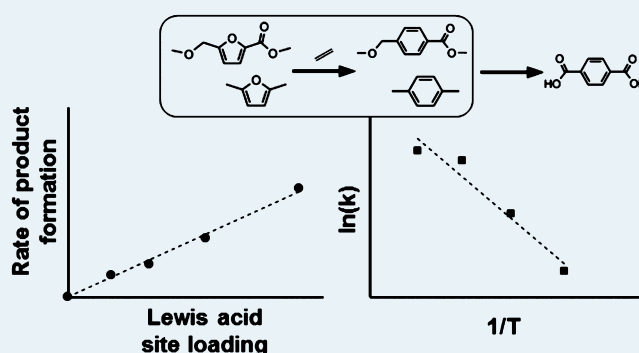
1. INTRODUCTION

The current commercial route to "green" polyethylene terephthalate (PET) involves bioethanol-based ethylene glycol, resulting in PET that is ∼30 wt % renewable; the terephthalic acid (PTA) component is still made by liquid-phase oxidation of petroleum-derived p-xylene (PX).[1,2] Approximately 47 million tons of PTA was consumed globally in 2012.[3] There is strong interest in 100% renewable PET, and therefore, finding new technologies for the synthesis of renewable PTA has become an important area of research;[4−18] current technologies have recently been reviewed by Collias et al.[3]

We recently reported a new route to biobased PTA starting from the biomass-derived platform chemical, 5-hydroxymethyl-furfural (HMF).[18] This route utilizes new, selective Diels−Alder reactions with ethylene and offers major advantages over the previously proposed Diels−Alder routes to PX from HMF, which require a wasteful prereduction to 2,5-dimethylfuran (DMF) with H$_2$. Specifically, reaction of ethylene with either partially oxidized HMF, 5-hydroxymethyl-2-furoic acid (HMFA), or the methanol-protected variant, methyl 5-(methoxymethyl)furan-2-carboxylate

(MMFC), in the presence of silica molecular sieves having the zeolite beta topology and containing Lewis acid metal centers incorporated into the framework (e.g., Sn-β, Zr-β), affords 4-(hydroxymethyl)benzoic acid (HMBA) or methyl 4-(methoxymethyl)benzene carboxylate (MMBC), respectively.[18] We showed that the synthesis of MMBC from MMFC can be achieved with high selectivity (>70%) at ∼20−40% conversion with Zr-β as catalyst. Because HMFA can be produced easily and quantitatively from HMF[19] and the HMBA/MMBC oxidation step to the PTA/DMT monomers should be considerably easier than the corresponding oxidation of PX, this route offers the potential to produce entirely biobased PTA with high overall selectivity and lower costs compared with the previously proposed routes to PTA via DMF and PX.[20]
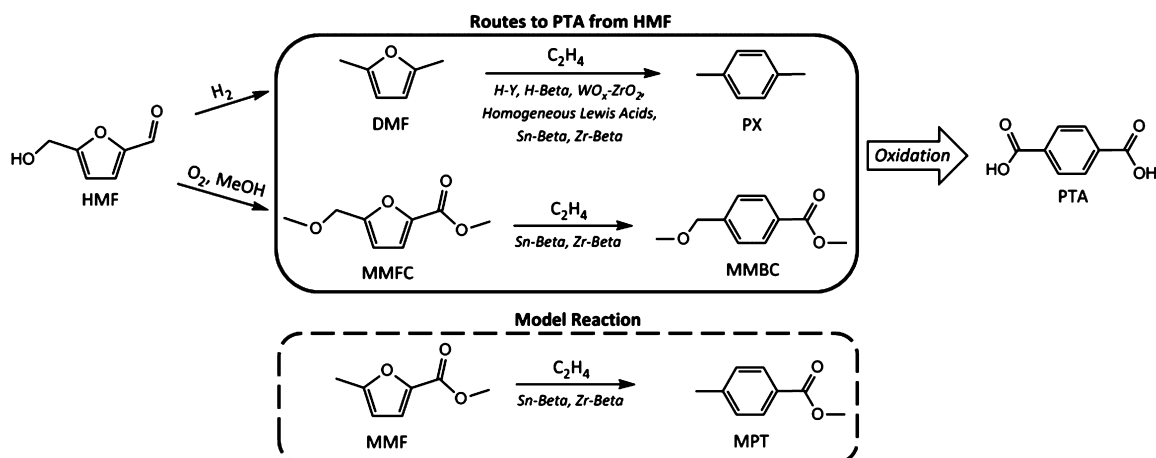
Previous experimental investigations on the synthesis of PX from DMF and ethylene using Bronsted acid zeolites

Scheme 1. Routes to PTA from HMF via the Ethylene Diels−Alder Dehydration of DMF or MMFC and the Ethylene Diels-Alder Dehydration of MMF As a Model Reaction

(i.e., H−Y, H-*β*)[5,7−9,12] or WO_x−ZrO_2[13] as catalysts have reported kinetic data such as turnover rates and apparent activation energies and proposed an overall reaction pathway (for H−Y) based on identification of a number of side products.[6] Catalysis by extraframework alkali cation (Li⁺, Na⁺, etc.) Lewis acid centers in zeolites Y and Beta have also been studied in a theoretical investigation that provided calculated energy profiles for the DMF/PX system.[10]

Here, we report the use of silica molecular sieve catalysts containing framework Lewis acid centers (e.g., Sn-*β*, Zr-*β*) for the synthesis of PX, MMBC and methyl *p*-toluate (MPT) by reacting DMF, MMFC, and methyl 5-methyl-2-furoate (MMF), respectively, with ethylene. The reactions in this study are summarized in Scheme 1; the MMF/MPT system is considered only as a model reaction, whereas the DMF/PX and MMFC/MMBC systems are potentially important routes for production of PTA from HMF. We propose a reaction pathway for the synthesis of MMBC from MMFC by identifying key side products using ¹H NMR analysis and gas chromatography/time-of-flight mass spectroscopy (GC/TOF-MS). Next, experiments using Zr-*β* catalysts of varying Si/Zr ratios are examined to determine the possible effect of mass transport on rates of product formation in the DMF/PX and MMF/MPT systems (using the Madon−Boudart methodology[21]), followed by measurements of apparent activation energies (E_a's). Finally, ¹³C kinetic isotope effects (KIEs) are calculated for the MMF/MPT and MMFC/MMBC systems by measuring changes in the overall ¹³C/¹²C ratio of the furanic dienes by gas chromatography/isotope ratio mass spectrometry (GC/IR-MS) in reactant-depletion experiments.

2. EXPERIMENTAL METHODS

2.1. Preparation of Catalyst Materials. Zr-*β* molecular sieve was prepared as follows: 7.46 g of an aqueous tetra-ethylammonium hydroxide (TEAOH) solution [Sigma-Aldrich, 35% (w/w)] was diluted with 15 g of water. A 6.98 g portion of tetraethylorthosilicate (TEOS) [Sigma-Aldrich, 98% (w/w)] was added, and the mixture was stirred on a magnetic stirplate until it became a single phase. A separate solution was prepared by diluting zirconium(IV) propoxide [Sigma-Aldrich, 70% (w/w) in propanol] in 2 g of ethanol, and this solution was added dropwise to the first solution with stirring. Samples with gel Si/Zr = 63−400 were prepared. The resulting mixture was

covered and stirred overnight to allow complete hydrolysis of the TEOS. The desired water ratio in the gel was obtained by complete evaporation of ethanol, propanol, and some water. The gel was transferred to a Teflon liner before 0.739 g of hydrofluoric acid (HF) solution [Sigma-Aldrich, 48% (w/w)] was added, resulting in a thick gel with a composition of SiO_2/0.003−0.016 ZrO_2/0.54 TEAOH/0.54 HF/6.75 H_2O. Finally, 0.6 g of a mixture of dealuminated zeolite Beta crystals in water, prepared according to the method reported by Chang et al.,[22] was added to the gel. The Teflon liner was sealed in a stainless steel autoclave and heated at 140 °C under rotating conditions for 5−7 days. The solids were recovered by centrifugation, washed with water (3 times) and acetone (1 time), and dried at 100 °C overnight.

Sn-*β* molecular sieve was prepared as follows: 7.46 g of an aqueous TEAOH solution [Sigma-Aldrich, 35% (w/w)] was diluted with 15 g of water. A 6.98 g portion of TEOS [Sigma-Aldrich, 98% (w/w)] was added, and the mixture was stirred on a magnetic stirplate until it became a single phase. A separate solution was prepared by dissolving 0.094 g of tin(IV) chloride pentahydrate (SnCl_4·5H_2O) [Sigma-Aldrich, 98% (w/w)] in 1 g of water, and this solution was added dropwise to the first solution with stirring. The resulting mixture was covered and stirred overnight to allow complete hydrolysis of the TEOS. The following day, the desired water ratio in the gel was obtained by complete evaporation of ethanol and some water. The gel was transferred to a Teflon liner before 0.739 g of HF solution [Sigma-Aldrich, 48% (w/w)] was added, resulting in a thick gel with a composition of SiO_2/0.01 SnCl_4/0.54 TEAOH/0.54 HF/6.75 H_2O. Finally, 0.6 g of a mixture of dealuminated zeolite Beta crystals in water, prepared according to the method reported by Chang et al.,[22] was added to the gel. The Teflon liner was sealed in a stainless steel autoclave and heated at 140 °C under rotating conditions for 7 days. The solids were recovered by centrifugation, washed with water (3 times) and acetone (1 time), and dried at 100 °C overnight.

2.2. Characterization of Materials. Powder X-ray diffraction (XRD) patterns of the synthesized materials confirmed the Beta topology and indicated high crystallinity of the samples. XRD patterns were collected using a Rigaku Miniflex II diffractometer and Cu K*α* radiation. XRD patterns are provided in the Supporting Information (Figures S.1, S.2).

Scanning electron microscopy (SEM) images were recorded on a LEO 1550 VP FE SEM at an electron high tension (EHT)

of 15 or 20 kV and used to determine crystal size. SEM images are provided in the Supporting Informaion (Figures S.3–S.6).

Silicon/metal (Si/M) molar ratios were determined by Galbraith Laboratories (GLI procedure ME-70).

2.3. Procedure for Diels−Alder Dehydration Reactions Using Ethylene. Experiments were carried out in a 50 mL high-pressure stainless steel batch reactor (Parr Series 4590) equipped with a magnetic stirrer and heater. The reactor setup allowed for ethylene gas (Matheson, 99.995% purity) or helium to be charged to the reactor. In a typical experiment, 10 g of a 0.1 M diene [DMF (Sigma-Aldrich, 99%), MMF (Sigma-Aldrich, 97%), or MMFC (Enamine, 95%)] solution in dioxane (Sigma-Aldrich, 99.8%) and catalyst were loaded into the reactor. For reactions quantified by GC/FID, triglyme (Sigma-Aldrich, 99%) internal standard was also added at 0.1 M concentration. The magnetic stirrer was operated at 200 rpm, and the head space of the reactor was purged with helium gas with a fill/vent cycle (10 times). Next, the reactor was pressurized to 37 bar (room temperature) with ethylene gas, the inlet valve was closed, and the reaction was performed in batch operation. The reactor was heated to reaction temperature (170−230 °C) while the pressure increased autogenously (~60−80 bar). At the end of the reaction time, the reactor was allowed to cool to room temperature, and the reactor gases were vented. The product was then collected for analysis.

MMFC and MMF reaction experiments for the ^{13}C KIE study were performed with larger reaction solutions and catalyst amounts because multiple aliquots were taken during these experiments. For the MMFC reaction, 12 g of a 0.1 M MMFC solution and 100 mg of Zr-β were charged to the reactor; for the MMF reaction, 14 g of a 0.1 M MMF solution and 140 mg of Zr-β were charged to the reactor. Aliquots (~0.5 g) for ^{1}H NMR and GC/IR-MS analysis were collected at various time points by cooling and opening the reactor. When an aliquot was collected, the spent catalyst was removed from the reaction solution by centrifugation, an equivalent amount (100 mg for the MMFC reaction or 140 mg for the MMF reaction) of freshly calcined Zr-β was added, and the reactor was started again using the described protocol.

2.4. Analysis of Reaction Products by ^{1}H NMR. Reaction results were quantified by ^{1}H NMR as follows: 0.2 g of the starting diene solution and product solution were added to separate 1 g DMSO-d_6 solutions containing 5 mM tetraethylsilane as an internal standard. The two mixtures were transferred through filtering pipettes into NMR tubes, and the ^{1}H NMR spectra were collected at room temperature. By comparison with the tetraethylsilane peak, the concentrations could be determined, and conversions and yields were calculated. For example, the signals used for calculating the conversion of MMFC and the yield of MMBC: tetraethylsilane δ = 0.49 ppm (q, 8 H); MMFC δ = 4.42 ppm (s, 2 H), δ = 6.63 ppm (d, 1 H), and δ = 7.26 ppm (d, 1 H); MMBC δ = 4.50 ppm (s, 2 H), δ = 7.46 ppm (d, 2 H), and δ = 7.95 ppm (d, 2 H).

2.5. Analysis of Reaction Products by GC/FID. GC/FID analysis was performed on an Agilent 7890B GC system equipped with a flame ionization detector (FID). The column used was an Agilent HP-5 (30 m × 0.32 mm × 0.25 μm) with N_2 as carrier gas (6 mL/min flow through column). Samples were typically prepared for injection by filtering a small aliquot of the product solution through a filter pipet before diluting in dichloromethane (DCM) in a ratio of 30 mg sample:170 mg of DCM. Volumes of 1 μL were injected into the GC using a

Hamilton 5 μL GC injection syringe. Split injection mode was used with a 7:1 split ratio. A typical oven temperature program was as follows: Hold 75 °C for 0.3 min, ramp to 90 °C at 10 °C/min and hold for 4.5 min, ramp to 300 °C at 50 °C/min and hold for 3 min.

2.6. Analysis of reaction products by GC/MS. GC/MS analysis was performed on an Agilent 5890 GC interfaced with a 5970 Mass Selective Detector. The column used was an DB-5 (30 m × 0.25 mm × 0.25 μm). The MSD was set to scan 50 to 550 m/z at 1.61 scans/s. The ionization mode was electron ionization, and the instrument was tuned using standard manufacturer autotune procedures using PFTBA (perfluoro-tributylamine).

GC/TOF-MS analysis was performed by JEOL on a AccuTOF GCv 4G system. The MS ion source was a EI/FI/FD Combination Ion Source (EI+: 70 eV, 300 μA, 280 °C. FI+: −10 kV, 40 mA(30 ms). JEOL emitter, heater off). A GC interface temperature of 280 °C was used with 1 Hz data acquisition rate.

2.7. Separation of Product Mixtures by Thin Layer Chromatography. Preparatory thin-layer chromatography (prep-TLC) on silica-gel plates was used to separate reaction product mixtures. The product mixture was filtered to remove spent catalyst, and the solution was deposited onto silica plates using a needle syringe. Using a 1 ethyl acetate/3 hexanes v/v mobile phase, the product mixture was separated into multiple bands (visible under UV light). Analytes in each band were collected by scraping the silica from the plates and extracting with dichloromethane (DCM); the DCM was then filtered and analyzed by GC/MS and GC/FID. If ^{1}H NMR analysis was desired, the DCM was removed by rotary evaporation, the residual organics redissolved in CDCl$_3$ NMR solvent, and a NMR spectrum was collected at room temperature.

2.8. GC/Isotope Ratio MS Experiments. Carbon isotope ratios (^{13}C/^{12}C) of analytes were determined using a ThermoFinnigan TraceGC Ultra connected to a Delta[plus] XP isotope-ratio mass spectrometer (IRMS) via the ThermoFinnigan GC Combustion-III interface. Principle of operation of this system is described by Sessions.[23] Briefly, analytes in the GC effluent are continuously combusted to CO_2, which is dried over a Nafion membrane then passed to the mass spectrometer. Multicollector monitoring of m/z 45/44 then provides high-precision measurement of the ^{13}C/^{12}C ratio, which is calibrated to the international VPDB scale by comparison to a lab CO_2 working gas standard.

Analytes were injected using a programmable-temperature vaporization (PTV) injector operated in programmed temperature mode (65 to 350 °C at 14.6°/s), and separated on a Zebron ZB-5 ms column (30 m × 0.25 mm × 1.00 μm) with He carrier gas at 1.4 mL/min. The oven temperature program was 100 °C for 0.2 min, 7°/min up to 150°, 20°/min up to 310°, with a hold at 310 °C for 4 min. Analytes were oxidized to CO_2 in a reactor containing CuO, Ag, and Pt wires that was reoxidized with O_2 every night. [13]C/^{12}C ratios were calibrated via CO_2 reference gas peaks inserted at the beginning and end of every chromatogram. Data were collected at 8 Hz and processed using Isodat v2.1 software. Precision of replicate measurements of unknowns averaged ±5.8 ppm for the ^{13}C/^{12}C ratio of MMF (0.5‰ in δ ^{13}C value), and ±1.3 ppm for MMFC (0.11‰ in δ ^{13}C). Accuracy, measured as the mean error for an external standard mixture containing eight fatty acid methyl esters, was 3.5 ppm in ^{13}C/^{12}C ratio (0.31‰ in δ ^{13}C value).

3. RESULTS AND DISCUSSION

3.1. Identification of Side Products in the Synthesis of MMBC from MMFC and C$_2$H$_4$.

MMFC was reacted with ethylene in the presence of Zr-β and Sn-β under the previously reported reaction conditions.[18] The product solutions were analyzed by GC/FID to determine the number of side products being produced using both the Zr-β and Sn-β catalysts. The chromatograms, along with the reaction results (conversion, yield, and selectivity), are shown in Figure 1.
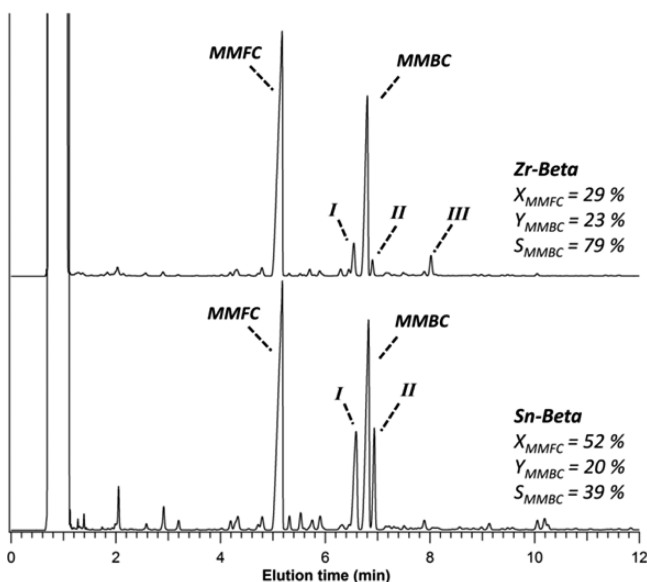

Figure 1. GC/FID chromatograms of product solutions in the Diels−Alder dehydration reaction of MMFC and ethylene using Zr-β (Si/Zr = 92) and Sn-β (Si/Sn = 129). Reaction conditions: 0.1 M MMFC in dioxane, 100 mg catalyst, 190 °C, 70 bar C$_2$H$_4$, 6 h. Conversions (X) and yields (Y) determined by ^{1}H NMR, and selectivity (S) is calculated by Y/X.

The largest side product peaks in the Zr-β chromatogram are designated as compounds **I**, **II**, and **III**. In the Sn-β system, products with the same elution times also appeared along with many additional side products. Notably, considerably more of compounds **I** and **II** are produced by the Sn-β than the Zr-β catalyst.

The product solutions from the Sn-β and Zr-β catalysts were analyzed by GC/MS, giving molecular weights for compounds **I**, **II**, and **III** as 166, 194, and 194, respectively, and confirming that **I** and **II** are the same for both catalysts. No matches were found for any of the three in MS libraries of known compounds. The mass spectra for the compounds are provided in the Supporting Information (Figures S.7−S.9). Prep-TLC was used to separate the reaction product mixtures in an effort to isolate the unknown side products for further analysis; since larger amounts of products **I** and **II** were produced using Sn-β as catalyst, that product solution was used. One of the TLC bands contained essentially only MMFC and compound **I**, according to both GC/MS and GC/FID (Figure S.10). Several TLC plates provided enough sample to obtain a ^{1}H NMR spectrum (Figure S.11).

The obtained MS pattern and ^{1}H NMR spectrum support the assignment of compound **I** as a cyclohexadiene compound, methyl 4-formylcyclohexa-1,3-diene-1-carboxylate (Figure 2). Each of the protons in this structure is in agreement with the
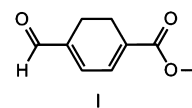

Figure 2. Proposed molecular structure of compound **I**, methyl 4-formylcyclohexa-1,3-diene-1-carboxylate.

relative areas and chemical shifts of the six numbered peaks in the NMR spectrum (Table S.1), and the MS fragmentation pattern is also consistent with this structure.

The TLC method also yielded a fraction containing side product **II** (confirmed by GC/FID and GC/MS), although several other compounds were also present, and insufficient material was collected for a satisfactory ^{1}H NMR spectrum.

To provide additional information for identifying the side products, more accurate fragment masses and chemical formula predictions were obtained by TOF-MS analysis. The electron ionization TOF-MS patterns are provided for compounds **I** and **II** (Figure S.12); m/z (to the nearest thousandth) for the parent ions of compounds **I** and **II** are 166.063 and 194.094, respectively, corresponding to chemical formulas of C$_9$H$_{10}$O$_3$ and C$_{11}$H$_{14}$O$_3$. The former (C$_9$H$_{10}$O$_3$) matches the structure of compound **I** on the basis of the ^{1}H NMR spectrum.

Comparing the mass spectra (Figure S.12), it is clear that the masses of all the fragments in the two spectra are very similar, if not identical. In addition, the difference in the predicted chemical formulas is equivalent to one ethylene molecule (C$_2$H$_4$), and the first fragment peak in the mass spectrum of compound **II** (166.063) corresponds to a loss of one ethylene molecule. This suggests a close relationship between the two compounds, most probably that compound **II** results from addition of ethylene to compound **I**. Because the proposed structure of compound **I** contains a cyclohexadiene functionality, it seems reasonable to propose that compound **II** is the Diels−Alder adduct of compound **I** and ethylene, methyl 4-formylbicyclo[2.2.2]oct-2-ene-1-carboxylate (Figure 3).
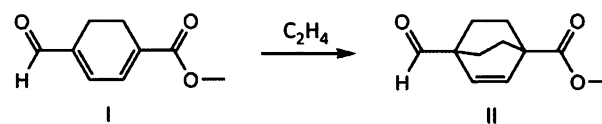

Figure 3. Proposed molecular structure of compound **II**, methyl 4-formylbicyclo[2.2.2]oct-2-ene-1-carboxylate, and its formation by reaction of compound **I** with C$_2$H$_4$.

A retro-Diels−Alder reaction to produce ethylene and compound **I** could be expected to be facile during ionization in the MS, to produce a fragmentation pattern similar to compound **I**. Such a relationship between the mass spectra of a cyclohexadiene and its Diels−Alder adduct with ethylene has been seen in other examples (i.e., 1,3-cyclohexadiene and bicyclo[2.2.2]oct-2-ene[24]). The formation of a bicyclo[2.2.2]-oct-2-ene from the Diels−Alder addition of ethylene to a cyclohexadiene side product was also observed by Do et al. in the reaction of DMF and ethylene to PX (Figure S.13).[6]

Reanalysis of the Sn-β- and Zr-β-catalyzed product solutions after several weeks of storage in vials at ambient conditions revealed the formation of new side products: in addition to MMFC and MMBC, methyl 4-formyl benzoate (MFB), dimethyl 2,5-furandicarboxylate (DMFC), and dimethyl terephthalate (DMT) were the main species observed by GC/FID (Figure 4). The assignments were confirmed

by GC/MS (Figures S.14–S.16). During the formation of these new species, the original side products, methyl
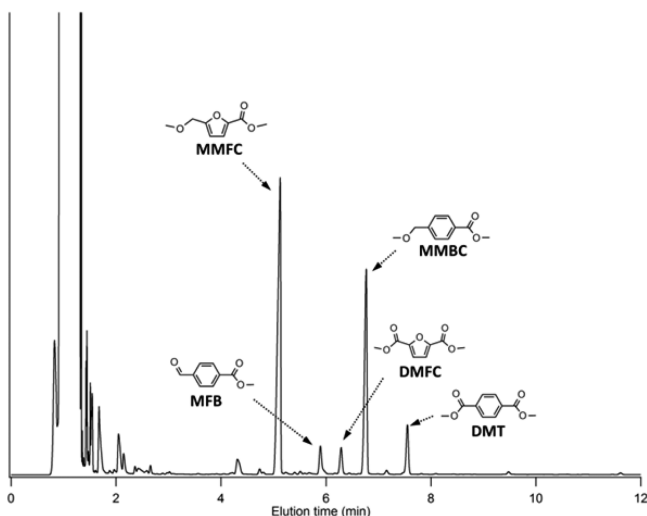

Figure 4. GC/FID chromatogram of MMFC-ethylene Diels−Alder product solution using Zr-β after storing for several weeks at room temperature.
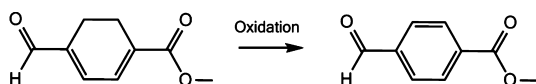

Figure 5. Proposed oxidation of methyl 4-formylcyclohexa-1,3-diene-1-carboxylate to methyl 4-formyl benzoate (MFB) under ambient conditions.
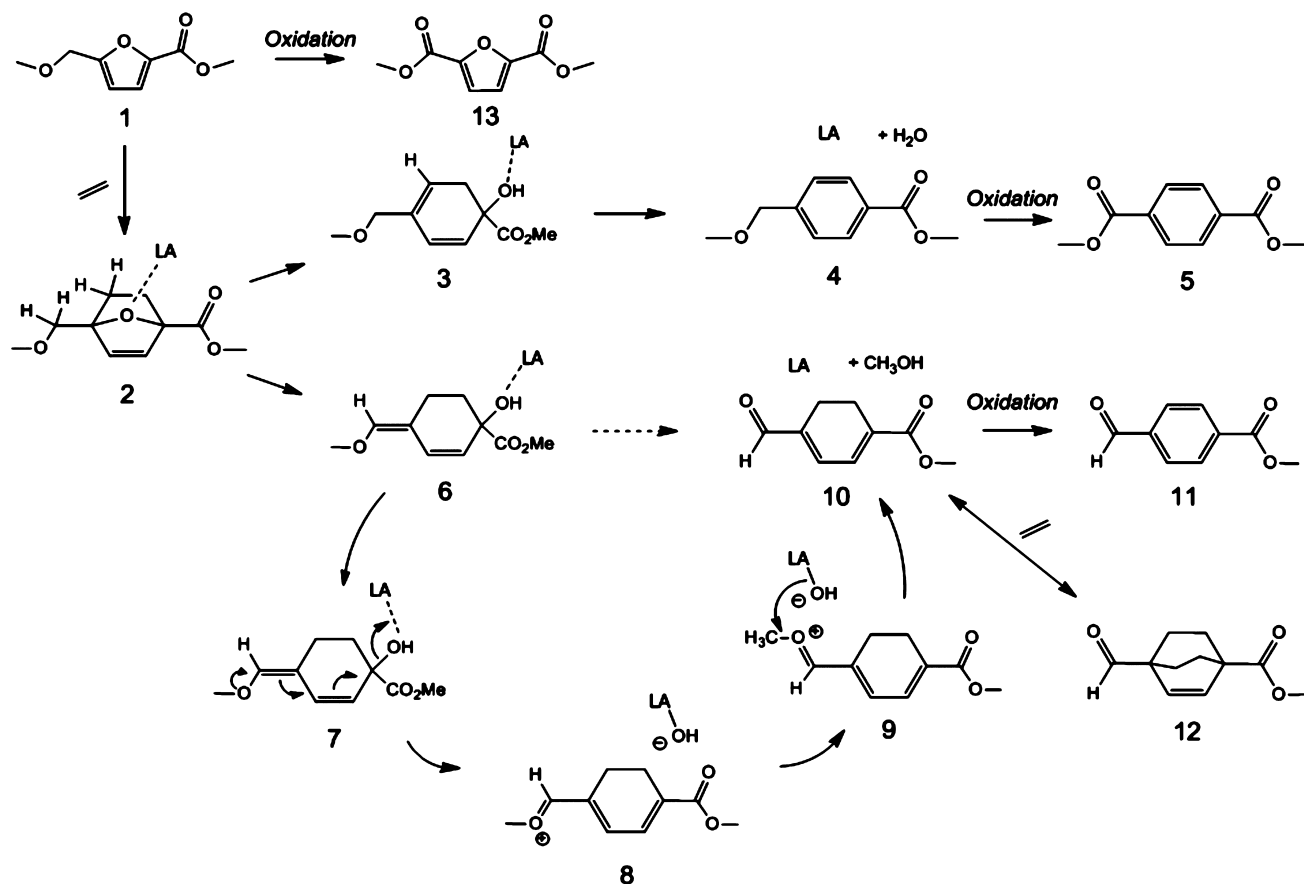
4-formylcyclohexa-1,3-diene-1-carboxylate and methyl 4-formylbicyclo[2.2.2]oct-2-ene-1-carboxylate, disappeared.

It is highly probable that MFB forms by autoxidative dehydrogenation of methyl 4-formylcyclohexa-1,3-di-carboxylate, as shown in Figure 5; similar oxidations of cyclohexadienes to aromatics have been reported (Figures S.17, S.18).[6,25] DMFC and DMT likely arise from the oxidation of MMFC and MMBC, respectively.

Because the oxidation of MFB to monomethyl terephthalate is expected to be relatively facile, the main side products, methyl 4-formylcyclohexa-1,3-diene-1-carboxylate and methyl 4-formylbicyclo[2.2.2]oct-2-ene-1-carboxylate, are not necessarily undesired side products and may be included when measuring the overall selectivity of the system for the production of PTA precursors (i.e., MMBC, MFB) from MMFC and ethylene.

In the current commercial process for PX oxidation to PTA, a significant cost is incurred from the oxidation of acetic acid solvent (solvent burning) under the severe oxidation conditions required.[1] Here, the PTA precursors (e.g., MMBC, MFB) should require less severe oxidation conditions for PTA synthesis, so solvent burning would be minimized. This may be an important consideration when comparing the overall economics of this route with those producing PX as the intermediate to renewable PTA.

3.2. Overall Reaction Pathway for the Synthesis of MMBC from MMFC and C$_2$H$_4$. Our proposed overall reaction network for the system is shown in Figure 6. The Lewis acid catalyst is involved in catalyzing the Diels−Alder dehydration of MMFC (**1**) and ethylene to MMBC (**4**) via the ring-opened

Figure 6. Proposed reaction network for the Diels−Alder dehydration of MMFC and ethylene to MMBC with Zr-β and Sn-β.

Diels–Alder adduct **3**. The formation of compound **I**, methyl 4-formylcyclohexa-1,3-diene-1-carboxylate (**10**), could also be formed via a Lewis acid-catalyzed pathway. One possible mechanism for the formation of **10** involves an alternate ring-opened Diels–Alder adduct (**6**) and the elimination of methanol. The product **10** then reacts with ethylene to form the compound **II** (**12**). The conversion of **10** to **12** is expected to be reversible, so as **10** oxidizes to form **11**, both **10** and **12** are consumed. This would reasonably explain the formation of **11** at the expense of **10** and **12** in the GC chromatogram after the solutions are stored for long times. DMFC (**13**) and DMT (**5**) are likely formed from the oxidation of MMFC (**1**) and MMBC (**4**), respectively, while being stored at room temperature. Alternate acid-catalyzed pathways for the ring-opening of the Diels–Alder adduct have also been proposed or observed in recent investigations on a DMF/PX system using Bronsted acid zeolite catalysts (Figure S.19).[6,11]

3.3. Reaction Kinetics Experiments for the Madon–Boudart Test.
Diels–Alder dehydration reactions catalyzed by the Lewis acid molecular sieve, Zr-β, were conducted for (1) the synthesis of PX from DMF and ethylene and (2) the synthesis of MPT from MMF and ethylene.

For each system, the observed reaction kinetics of the Diels–Alder dehydration reactions were tested for the influence of mass and heat transfer limitations within the molecular sieve catalysts. This was accomplished by performing the Madon–Boudart test, which involves correlating the initial rates of product formation versus varying active site (Zr) content in the catalyst. The Madon–Boudart criterion states that if the initial

rates are linear with the number of active sites in different catalyst samples of constant crystal size and number, then the transport of the reactant molecule to the catalytic active site is not limiting the rate of reaction.[21] It is critical to determine whether transport limitations are present before measuring the activation barriers for the reactions. If transport of the reactant to the active sites is limiting the rate, any measured activation energy will not be representative of the chemical reaction.

A series of four Zr-β samples of varying Si/Zr molar ratios were prepared. Table 1 summarizes the Si/Zr ratios and crystal size of each sample. PX and MPT yield profiles using the four Zr-β catalysts were collected at 230 °C and are shown in Figure 7.

To determine whether transport limitations within the microporous Zr-β catalysts were influencing the rate of product synthesis, the initial rates of PX and MPT synthesis were plotted against the total Zr content (mmol Zr) present in the catalyst (Figure 8) to generate Madon–Boudart plots. The initial rates were determined by estimating the slope of the yield profiles at $t = 0$. Details on the method used in reporting the initial rates and error bars from the yield profiles are provided in the Supporting Information (Figures S.20, S.21).

The initial rate of PX production is clearly linear and proportional to the Zr content in the catalyst (Figure 8, top). This result shows that transport limitations are not influencing the measured kinetics at temperatures up to 230 °C. In addition, it indicates that all the Zr atoms are incorporated into the framework and are active catalytic sites, and that all the active sites in the crystals are accessible for catalysis.

In contrast, the plot of the initial rates for MPT production does not appear to pass through the origin (Figure 8, bottom), particularly when including the highest Zr content point (Zr-β-92), indicating a possible diffusion limitation. Because the rate for the catalyst with the lowest Zr content (Zr-β-492) has a relatively large uncertainty and the intermediate points (Zr-β-264 and Zr-β-155) appear to be collinear with the origin, a plausible interpretation may be that only the sample with the highest Zr content exhibits transport limitation.

3.4. Apparent Activation Energy (E_a) Measurements.
Because the synthesis of PX is not transport-limited in any of

Table 1. Zr-β Samples Used in Madon–Boudart Experiments[a]

sample name	Si/Zr atom ratio	crystal size (μm)
Zr-β-92	92	0.75−1.0
Zr-β-155	155	0.75−1.0
Zr-β-264	264	1.0−1.25
Zr-β-492	492	0.75−1.0

[a]Crystal size determined by SEM. Si/Zr molar ratios determined by Galbraith Laboratories (GLI procedure ME-70).
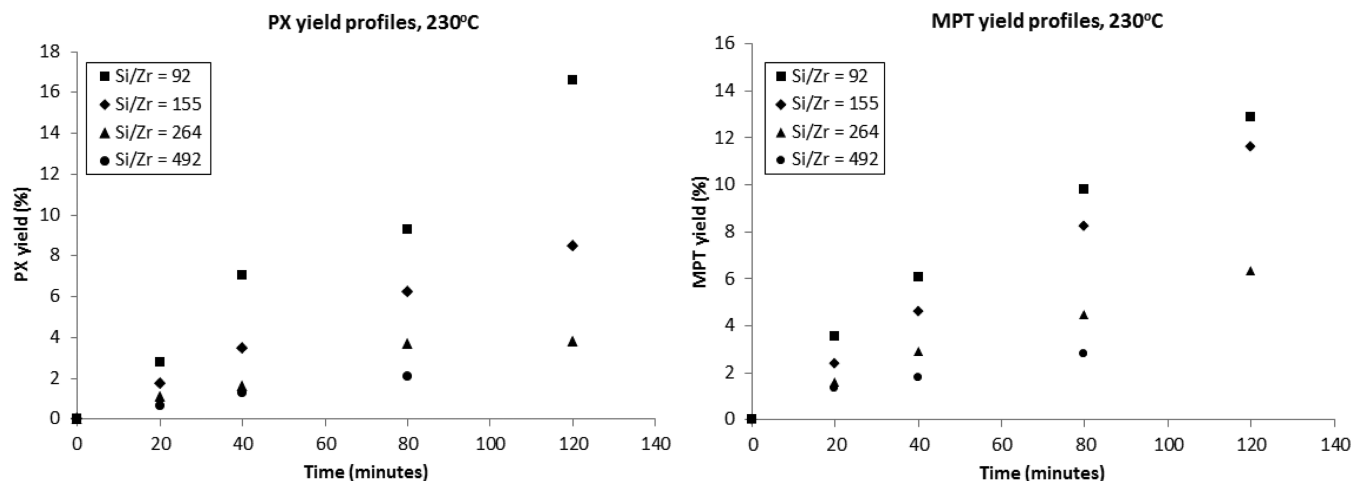

Figure 7. PX and MPT yield profiles for Diels–Alder dehydration of DMF and MMF, respectively, with ethylene using Zr-β catalysts with varying Si/Zr molar ratios. Reaction conditions for PX synthesis: 0.1 M DMF in dioxane, 0.1 M triglyme (internal standard), 30 mg of catalyst, 230 °C, 35 bar C_2H_4 (room temperature). Reaction conditions for MPT synthesis: 0.1 M MMF in dioxane, 0.1 M triglyme (internal standard), 100 mg of catalyst, 230 °C, 35 bar C_2H_4 (room temperature).
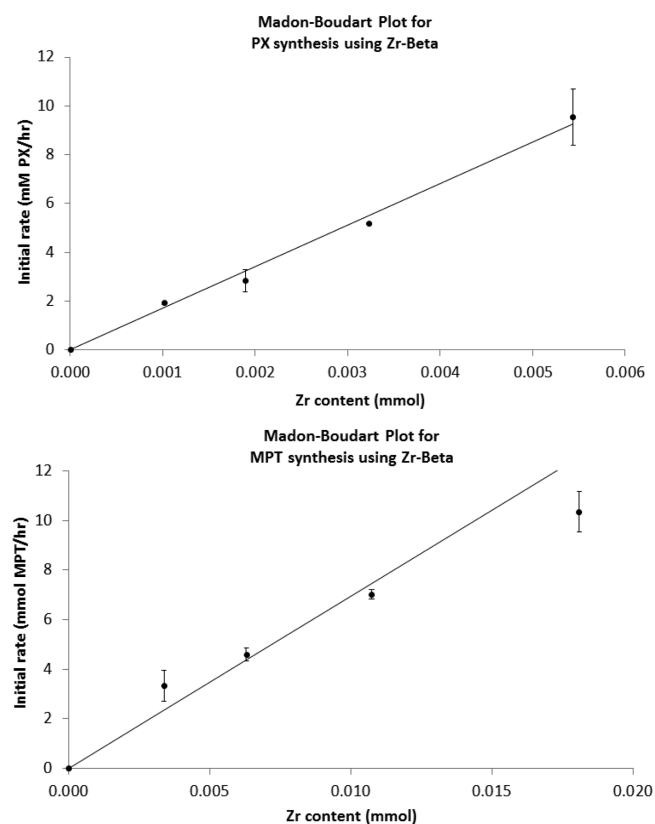
Figure 8. Madon−Boudart plots for Zr-β catalyzed PX (top) and MPT (bottom) synthesis at 230 °C.

Figure 10. Arrhenius plots for Zr-β catalyzed PX (top) and MPT (bottom) synthesis for 170−230 °C.

the Zr-β samples and the synthesis of MPT may be transport-limited only in the catalyst with the lowest Si/Zr ratio (Zr-β-92), apparent E_a's for the synthesis of PX and MPT were measured using the Zr-β-155 sample. The PX and MPT yield profiles were collected at temperatures between 170 and 230 °C (Figure 9). The initial product synthesis rates estimated from the profiles were used to generate Arrhenius plots (Figure 10).

The apparent E_a for the synthesis of PX appears to vary with reaction temperature. In the 170−210 °C range, the apparent E_a is 10.5 kcal/mol, but in the 210−230 °C range an apparent
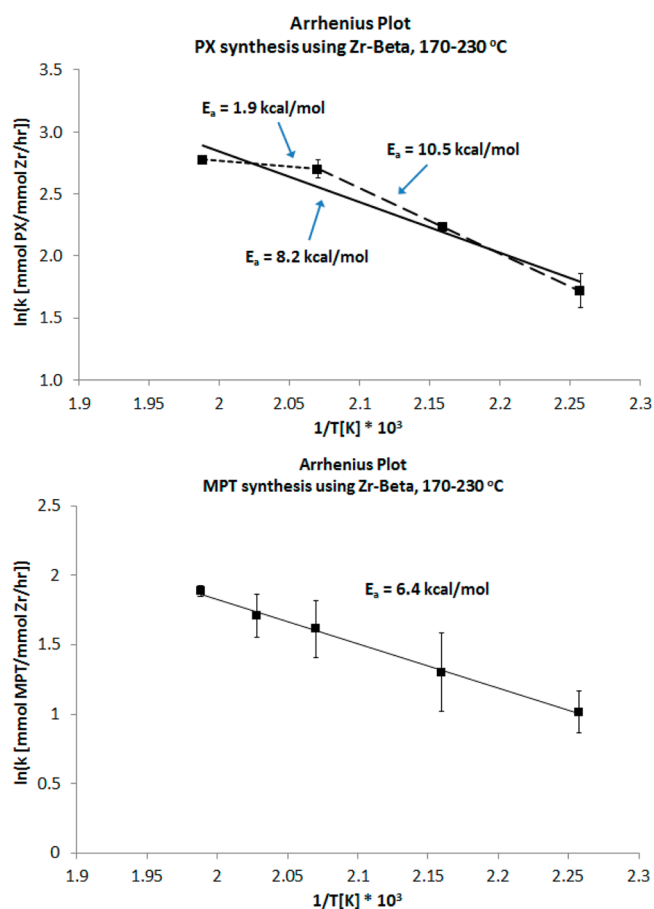
E_a of only 1.9 kcal/mol is measured. The average E_a for the entire 170−230 °C range is 8.2 kcal/mol. For the synthesis of MPT, the apparent E_a is 6.4 kcal/mol and constant within the 170−230 °C range.

Because all the E_a values are far too low to be the true activation energy of a single chemical step, these data suggest the apparent E_a consists of a group of terms that result in low
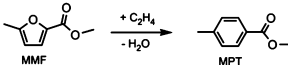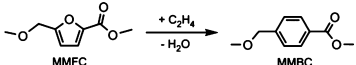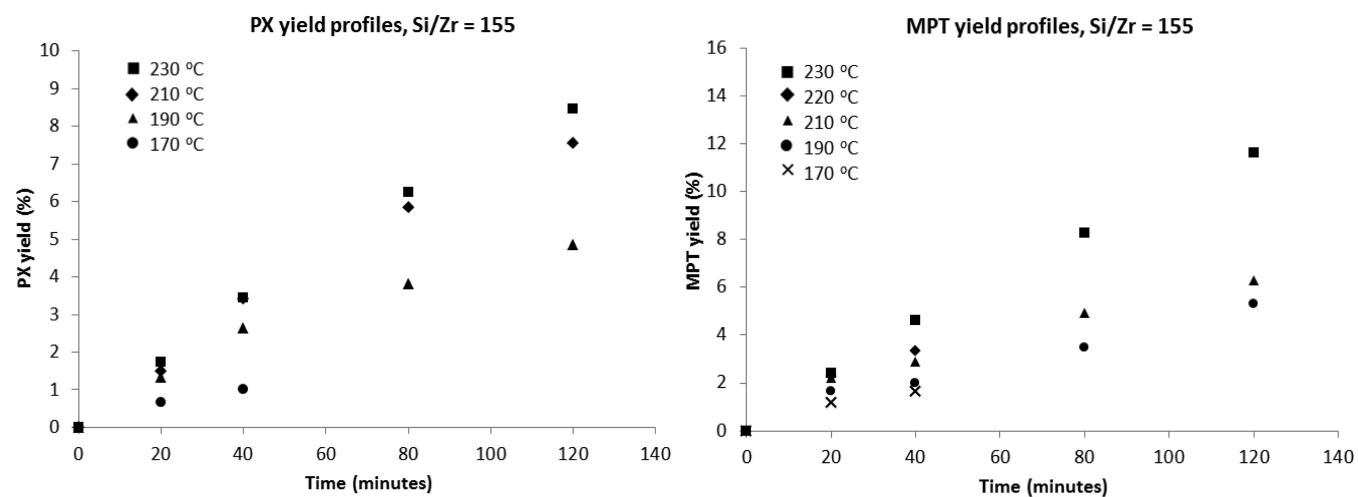

Figure 9. PX and MPT yield profiles for Diels−Alder dehydration of DMF and MMF, respectively, with ethylene using Zr-β-155. Reaction conditions for PX synthesis: 0.1 M MMF in dioxane, 0.1 M triglyme (internal standard), 30 mg of Zr-β-155, 35 bar C_2H_4 (room temperature). Reaction conditions for MPT synthesis: 0.1 M MMF in dioxane, 0.1 M triglyme (internal standard), 100 mg of Zr-β-155, 35 bar C_2H_4 (room temperature).

Table 2. Reaction Data for ^{13}C KIE Study: Synthesis of MPT and MMBC Using Zr-β^a

Reaction	Reaction time (hr)	Conversion (%)	Yield (%)	Product Selectivity (%)
MMF → MPT (+ C$_2$H$_4$, − H$_2$O)	22	41	42	103
	42	74	72	98
	66	85	81	96
MMFC → MMBC (+ C$_2$H$_4$, − H$_2$O)	24	39	30	76
	46	61	48	79
	70	73	53	73

^{a}Reaction conditions: 0.1 M MMF or MMFC in dioxane, Zr-β (~70 furan:Zr molar ratio), 190 °C, 70 bar C$_2$H$_4$. Conversions and yields determined by ^{1}H NMR, and product selectivity is calculated by yield/conversion.

overall values. Because two chemical reactions, Diels−Alder cycloaddition and dehydrative aromatization, take place in succession, with the first quite possibly in thermodynamic equilibrium, the measured apparent E_a may include the ΔH_{rxn} for the reversible Diels−Alder cycloaddition, the actual E_a for the dehydrative aromatization of the Diels−Alder adduct, and perhaps other terms, such as reversible adsorption of reactants, intermediates, and products onto the catalyst (ΔH_{ads}). In the simplest scenario, the Diels−Alder cycloaddition is in fast equilibrium, followed by a rate-determining dehydration step, and all ΔH_{ads} terms are neglected. Here, the measured E_a would be the sum of ΔH_{rxn} for the reversible Diels−Alder reaction (exothermic) and the actual E_a for the rate-determining dehydration, but it is the latter that dictates the reaction temperature required for any product formation. As the temperature is increased, the rate of dehydration of the Diels−Alder adduct increases according to the true E_a of the dehydration, but the equilibrium of the Diels−Alder cyclo-addition shifts toward the reactants (Le Châtelier's principle) and results in a lower concentration of the Diels−Alder adduct. Overall, the rate increase is much less than the dehydration E_a would predict, and the measured apparent E_a is smaller. A recent investigation by Patet et al. on the Diels−Alder dehydration of DMF and ethylene to produce PX using a Bronsted acid H−Y zeolite catalyst in heptane solution showed a reaction regime in which the effective rate constant for the production of PX included multiple terms.[12]

3.5. ^{13}C Kinetic Isotope Effect (KIE) Measurements. The Madon−Boudart experiments clearly indicate that the Zr-β-catalyzed Diels−Alder dehydration reaction rate for the synthesis of PX is not diffusion-limited and suggested the same for the synthesis of MPT, although those results are less conclusive. Therefore, because the system is reaction-limited, the rate-limiting step should express a substantial kinetic isotope effect (KIE). The existence of such a KIE not only would confirm the findings from the Madon−Boudart experiments that the system is reaction-limited, but also may help provide further information regarding the mechanism of overall reaction. For example, a ^{13}C KIE is known to occur in Diels−Alder cycloadditions.[26,27]

Here, we designed a natural abundance ^{13}C reactant-depletion experiment using GC/isotope ratio mass spectrom-etry (GC/IR-MS) to measure changes in the overall ^{13}C/^{12}C ratio of the unreacted furan at different fractional conversions. This method is convenient because only a small amount of sample is needed (<1 nmol C) and the reaction products are readily separated by GC. However, because high-precision isotope ratio measurement requires conversion of the analyte to CO$_2$, KIE's for specific carbon positions within the molecule cannot be directly measured. Instead, we measured ^{13}C KIE

values for the whole reactant molecule, and calculated corresponding values for the 2- and 5-carbons of the furan ring by assuming that only these two carbons, which form the new C−C bonds with ethylene in the Diels−Alder dehydration reaction, are involved in the ^{13}C KIE.

The ^{13}C KIE analysis was performed on the MMF/MPT and MMFC/MMBC systems using Zr-β catalyst. High levels of conversion were achieved by running for long reaction times, and the reactor was stopped at intermediate times to collect small aliquots for analyses by ^{1}H NMR and GC/IR-MS. The results are summarized in Table 2, and the ^{13}C/^{12}C ratios of the remaining MMF and MMFC at different conversions are plotted in Figure 11. The GC/IR-MS results clearly show that

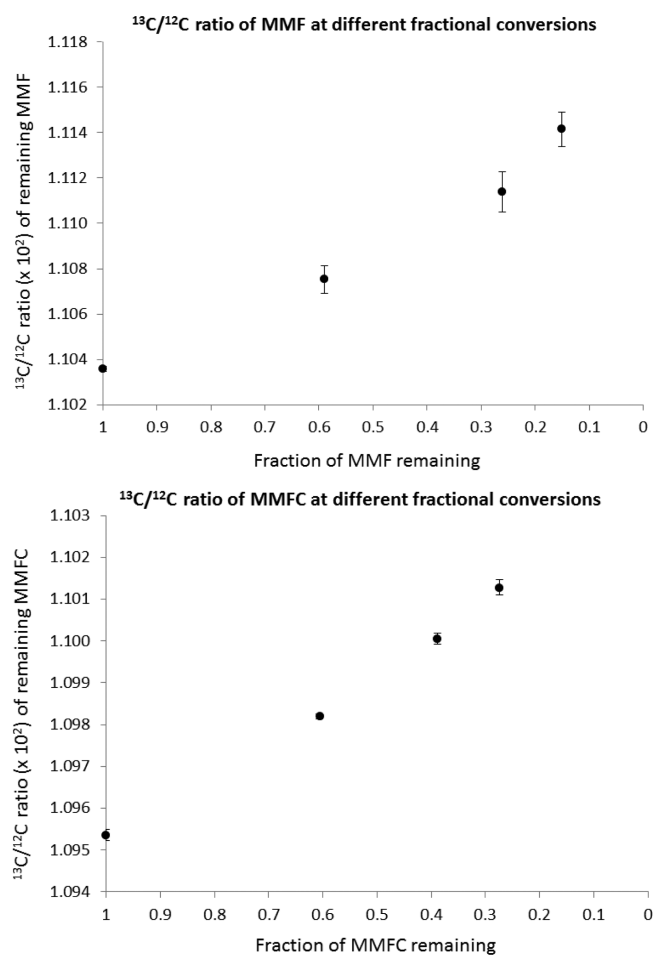**Figure 11.** ^{13}C/^{12}C ratios of remaining MMF and MMFC at different fractional conversions from reactions in Table 2.

the measured $^{13}C/^{12}C$ ratios of the unreacted furans in both systems (MMF/MPT and MMFC/MMBC) are increasing with conversion, indicating the presence of a substantial ^{13}C KIE for both reactions.

Table 3 lists the data plotted in Figure 11, the calculated $^{13}C/^{12}C$ ratios of the C-2 and C-5 carbons of the furan ring

Table 3. Calculated ^{13}C Compositions of 2- and 5-Position Carbons of Furan Ring Relative to the Starting Material (R/R_0), and the ^{13}C KIE Values Using Equation S.1[a]

reaction	fractional conversion of furan (F)	$^{13}C/^{12}C$ of unreacted furan ($\times 10^2$)	calcd ^{13}C composition of C-2, C-5 relative to starting material (R/R_e)	^{13}C KIE calculaed from R/R_e and eq S.l
MMF-MPT	0	1.1036 (1)		
	0.41 (2)	1.1075 (6)	1.013 (2)	1.024 (5)
	0.74 (2)	1.1114 (9)	1.025 (3)	1.019 (3)
	0.85 (2)	1.1142 (8)	1.034 (2)	1.018 (3)
MMFC-MMBC	0	1.0954 (1)		
	0.39 (2)	1.0982 (1)	1.010 (1)	1.021 (3)
	0.61 (2)	1.1001 (1)	1.017 (1)	1.018 (2)
	0.73 (2)	1.1013 (2)	1.022 (1)	1.017 (2)

[a]Uncertainty in the last digit is given in parentheses.

relative to their starting values (R/R_0), and the calculated ^{13}C KIE values from R/R_0 using eq S.1. Details of the calculations of R/R_0 are provided in the Supporting Information. The KIE values for both reaction systems are ~1.02 and are nearly constant with the extent of conversion, within experimental uncertainty. For the MMF/MPT system, the selectivities for the Diels−Alder dehydration product are high (>96%), and hence, the measured KIE arises solely from this reaction. In the MMFC/MMBC system, the selectivity for the Diels−Alder dehydration product is lower (73−79%), so the overall KIE value may be influenced by other reactions. In Sections 3.1 and 3.2, the identification of the main side products and side reactions for the Zr-β-catalyzed synthesis of MMBC showed that the main side products arise from an alternate dehydration pathway of the bicyclic Diels−Alder cycloadduct, so it is possible that the KIE is also being exhibited in the production of the side products, as well.

Because two reactions are occurring in tandem (Diels−Alder cycloaddition followed by dehydration), and both could result in a ^{13}C KIE, it is not possible to determine which reaction is rate-determining from these data. Previously reported ^{13}C KIE values for the Diels−Alder reaction between isoprene and maleic anhydride (1.017−1.022)[26] are very close to the values measured here, suggesting that the Diels−Alder cycloaddition between the furanic diene and ethylene is rate-determining; however, that conclusion does not appear consistent with the very low apparent activation energies. The main conclusion that *can* be drawn is that these findings are in agreement with the conclusion from the Madon−Boudart experiments, that the system is reaction-limited.

4. CONCLUSIONS

Two main side products in the Diels−Alder dehydration reaction between MMFC and ethylene using Sn- and Zr-β have been identified as a cyclohexadiene derivative, methyl 4-formylcyclohexa-1,3-diene-1-carboxylate, and its ethylene Diels−Alder product, methyl 4-formylbicyclo[2.2.2]oct-2-ene-1-carboxylate. Methyl 4-formylcyclohexa-1,3-diene-1-carboxylate is

a presursor to methyl 4-formyl benzoate (MFB) by autoxidative dehydrogenation. Because the oxidation of MFB to mono-methyl terephthalate should be relatively facile, these main side products are not necessarily undesired side products, and they should be included when calculating an overall selectivity to PTA precursors (MMBC, MFB, etc.) from HMF-derived MMFC.

Both Madon−Boudart experiments and ^{13}C KIE measurements indicate that these Diels−Alder dehydration processes (including each of the three systems studied here) using the pure Lewis acid Zr-β catalyst are reaction-limited and not transport-limited. The Madon−Boudart experiments also show that all the Zr atoms are active framework acid sites.

Once it was determined that the reaction system was not transport-limited, activation energies could be determined. Measurements for the two Diels−Alder dehydration systems, DMF/PX and MMF/MPT, catalyzed by Zr-β reveal low apparent E_a values that are too low to be activation energies of a single chemical step. Instead, these data suggest that the apparent E_a values represent a combination of terms that results in the low overall values. Because two reactions in tandem (Diels−Alder cycloaddition and dehydrative aromatization) occur over a heterogeneous catalyst, it is possible for the apparent E_a values to be a combination of terms that may include the ΔH_{rxn} for the reversible Diels−Alder reaction, the true E_a for the dehydrative aromatization of the Diels−Alder adduct, the ΔH_{ads} terms for adsorption steps in equilibrium (reactants or intermediates adsorbing reversibly onto the catalyst surface or active site), or others.

■ ASSOCIATED CONTENT

ⓢ Supporting Information

The Supporting Information is available free of charge on the ACS Publications website at DOI: 10.1021/acscatal.5b01309.

Catalyst characterization (X-ray diffractograms and SEM images), reaction product characterization (EI mass spectra and ^1H NMR), additional information on method for measuring initial reaction rates, and method for calculating R/R_0 values in Table 3 (PDF)

■ AUTHOR INFORMATION

Corresponding Author
*E-mail: mdavis@cheme.caltech.edu.

Present Address
§(J.J.P.) Zeolyst International Research & Development Center, 280 Cedar Grove Road, Conshohocken, PA 19428.

Notes
The authors declare no competing financial interest.

■ ACKNOWLEDGMENTS

■ REFERENCES

(1) Tomas, R. A. F.; Bordado, J. C. M.; Gomes, J. F. P. *Chem. Rev.* **2013**, *113*, 7421−7469.
(2) Landau, R.; Saffer, A. *Chem. Eng. Prog.* **1968**, *64*, 20−26.

(3) Collias, D. I.; Harris, A. M.; Nagpal, V.; Cottrell, I. W.; Schultheis, M. W. *Ind. Biotechnol.* **2014**, *10*, 91−105.

(4) Shiramizu, M.; Toste, F. D. *Chem. - Eur. J.* **2011**, *17*, 12452−12457.

(5) Williams, C. L.; Chang, C.-C.; Do, P.; Nikbin, N.; Caratzoulas, S.; Vlachos, D. G.; Lobo, R. F.; Fan, W.; Dauenhauer, P. J. *ACS Catal.* **2012**, *2*, 935−939.

(6) Do, P. T. M.; McAtee, J. R.; Watson, D. A.; Lobo, R. F. *ACS Catal.* **2013**, *3*, 41−46.

(7) Nikbin, N.; Do, P. T.; Caratzoulas, S.; Lobo, R. F.; Dauenhauer, P. J.; Vlachos, D. G. *J. Catal.* **2013**, *297*, 35−43.

(8) Xiong, R.; Sandler, S. I.; Vlachos, D. G.; Dauenhauer, P. J. *Green Chem.* **2014**, *16*, 4086−4091.

(9) Chang, C.-C.; Green, S. K.; Williams, C. L.; Dauenhauer, P. J.; Fan, W. *Green Chem.* **2014**, *16*, 585−588.

(10) Nikbin, N.; Feng, S.; Caratzoulas, S.; Vlachos, D. G. *J. Phys. Chem. C* **2014**, *118*, 24415−24424.

(11) Li, Y.-P.; Head-Gordon, M.; Bell, A. T. *J. Phys. Chem. C* **2014**, *118*, 22090−22095.

(12) Patet, R. E.; Nikbin, N.; Williams, C. L.; Green, S. K.; Chang, C.-C.; Fan, W.; Caratzoulas, S.; Dauenhauer, P. J.; Vlachos, D. G. *ACS Catal.* **2015**, *5*, 2367−2375.

(13) Wang, D.; Osmundsen, C. M.; Taarning, E.; Dumesic, J. A. *ChemCatChem* **2013**, *5*, 2044−2050.

(14) Wang, B.; Gruter, F. J. M.; Dam, M. A.; Kriegel, R. M. Process for the preparation of benzene derivatives from furan derivatives. Patent WO2014065657 A1, 2014.

(15) Gong, W. H. Terephthalic acid composition and process for the production thereof. U.S. Patent 8,299,278, 2012.

(16) Masuno, M. N.; Smith, P. B.; Hucul, D. A.; Dumitrascu, A.; Brune, K.; Smith, R. L.; Bissell, J.; Foster, M.; Methods of producing para-xylene and terephthalic acid. U.S. Patent Appl. No. 13/838,761, 2013.

(17) Brandvold, T. A. Carbohydrate route to para-xylene and terephthalic acid. U.S. Patent 8,314,267, 2012.

(18) Pacheco, J. J.; Davis, M. E. *Proc. Natl. Acad. Sci. U. S. A.* **2014**, *111*, 8363−8367.

(19) Casanova, O.; Iborra, S.; Corma, A. *ChemSusChem* **2009**, *2*, 1138−1144.

(20) Lin, Z.; Ierapetritou, M.; Nikolakis, V. *AIChE J.* **2013**, *59*, 2079−2087.

(21) Madon, R. J.; Boudart, M. *Ind. Eng. Chem. Fundam.* **1982**, *21*, 438−447.

(22) Chang, C.-C.; Wang, Z.; Dornath, P.; Cho, H. J.; Fan, W. *RSC Adv.* **2012**, *2*, 10475−10477.

(23) Sessions, A. L. *J. Sep. Sci.* **2006**, *29*, 1946−1961.

(24) Mass spectra available on webbook.nist.gov.

(25) Mcgraw, G. W.; Hemingway, R. W.; Ingram, L. L., Jr.; Canady, C. S.; Mcgraw, W. B. *Environ. Sci. Technol.* **1999**, *33*, 4029−4033.

(26) Singleton, D. A.; Thomas, A. A. *J. Am. Chem. Soc.* **1995**, *117*, 9357−9358.

(27) Singleton, D. A.; Schulmeier, B. E.; Hang, C.; Thomas, A. A.; Leung, S.-W.; Merrigan, S. R. *Tetrahedron* **2001**, *57*, 5149−5160.